RSC Advances

PAPER

View Article Online
View Journal | View Issue

Cite this: *RSC Adv.*, 2020, **10**, 25311

A CO_2-responsive smart fluid based on supramolecular assembly structures varying reversibly from vesicles to wormlike micelles†

Chunming Xiong,[ab] Falin Wei,[ab] Qiang Zhou,[ab] Kang Peng,*[ab] Zhengrong Ye[ab] and Haiyang Yang *[ab]

CO_2-responsive smart fluids have been widely investigated in the past decade. In this article, we reported a CO_2-responsive smart fluid based on supramolecular assembly structures varying from vesicles to wormlike micelles. Firstly, oleic acid and 3-dimethylaminopropylamine reacted to form a single-chain weak cationic surfactant with a tertiary amine head group, *N*-[3-(dimethylamino)propyl]oleamide (NDPO). Then, 1,3-dibromopropane was used as the spacer to react with NDPO to form a gemini cationic surfactant, trimethylene α,ω-bis(oleate amide propyl dimethyl ammonium bromide) (GCS). By controlling the feed ratio of 1,3-dibromopropane and NDPO, we found that the mixtures of GCS and NDPO with the molar ratio of 7 : 3 approximately could form vesicles in aqueous solution by supramolecular self-assembly. After bubbling CO_2, the tertiary amine of NDPO was protonated. The packing parameter of the mixed surfactants reduced accordingly, accompanied by the transition of aggregates from vesicles to wormlike micelles. As a result, the zero-shear viscosity of the solution increased by more than four orders in magnitude. When the solid content of GCS/NPDO mixtures was higher than 5 wt% in solution, the sample treated by CO_2 behaved as a gel over a wide frequency range with shear-thinning and self-healing properties. In addition, the sol–gel transition could be repeatedly and reversibly switched by cyclically bubbling CO_2 and N_2. Our effort may provide a new strategy for the design of CO_2-responsive smart fluids, fostering their use in a range of applications such as in enhanced oil recovery.

Received 29th April 2020
Accepted 25th June 2020

DOI: 10.1039/d0ra03854g

rsc.li/rsc-advances

Introduction

Smart non-Newtonian fluids that undergo physicochemical changes in response to external stimuli, such as pH, light, CO_2, temperature, ionic strength and electric and magnetic fields, had drawn much attention in recent years.[1–3] As a significant type of smart fluid, the molecular self-assembly of surfactants created different aggregates, such as sphere micelles, rod micelles, wormlike micelles, vesicles, and liquid crystals.[4–7] Among these, wormlike micelles (WLMs) had received considerable attention due to special behaviors like polymers. Owing to the entanglement of wormlike micelles, the aqueous solution showed higher viscosity, and excellent properties of breaking and reforming compared with polymers.[1,8–11] Such unique rheological properties gave them potential application in enhanced oil and gas recovery, drug delivery, clear fracturing fluid and so on.[12–14] Recently, the reversible viscoelasticity of wormlike micelles which responded to an external stimulus, such as light,[15] temperature,[16] pH,[17] CO_2 (ref. 18) and electric field,[19] had been investigated extensively.

CO_2-responsive smart fluids would have more significance in practical industry because CO_2 was a non-toxic, inexpensive, benign and abundant gas.[20] Moreover, using CO_2 as a trigger could lead to many switching cycles without the accumulation of by-products.[21] Up to now, according to the present research on CO_2-responsive smart fluids, most of them were based on wormlike micelles.[22–25] For example, Zhang *et al.* reported a CO_2-responsive anionic wormlike micelle fluid by introducing trimethylamine into sodium erucate. Trimethylamine was protonated into a protonated tertiary ammonium salt when CO_2 was bubbled. It facilitated the growth of micelles as a hydrotrope by screening electrostatic repulsion between the anionic head groups in sodium erucate molecules, resulting in the formation of wormlike micelles and viscoelasticity build-up.[26] Feng and his co-workers synthesized a cation surfactant containing primary and secondary amines. After bubbling CO_2, the primary amine reacted with CO_2 to generate an amphoteric charge. This changed the packing parameter (the geometry of

[a]*Research Institute of Science and Technology, China National Petroleum Corporation, Beijing, 100083, P. R. China*

[b]*CAS Key Laboratory of Soft Matter Chemistry, School of Chemistry and Materials Science, University of Science and Technology of China, Hefei, 230026, P. R. China. E-mail: yhy@ustc.edu.cn; pengkang@mail.ustc.edu.cn*

† Electronic supplementary information (ESI) available. See DOI: 10.1039/d0ra03854g

the self-organized structures can be predicted to a certain extent based on the concept of packing parameter,[1] and the amphiphilic compounds are expected to assemble into spherical aggregates when $p < 1/3$, wormlike micelles when $1/3 < p < 1/2$, and vesicles when $1/2 < p < 1$) of the surfactant assembly and induced the transition of aggregate from vesicles to wormlike micelles, which occurred a sol–gel transition macroscopically.[18] Feng and his co-workers fabricated a CO_2-switchable wormlike micellar system by using nerucamidopropyl-*N*,*N*-dimethylamine without any hydrotropes. Its viscoelasticity varied by five orders of magnitude after cyclically bubbling CO_2 and air, but the hydrophobicity of the system also leaded to its poor solubility before bubbling CO_2.[27]

Although CO_2-responsive smart fluids had gained a rapid development over the last few years, most systems focused on the compounding of single-chain cationic or anionic surfactants, and the gemini cation surfactant regulated by CO_2 had seldom been reported. A gemini cation surfactant (GCS) consisted of two conventional surfactant molecules, which was chemically bonded together by a spacer. Compared to conventional single-chain surfactants, the gemini surfactant could self-assemble at much lower concentrations and are superior in surface activity. Many kinds of gemini cation surfactants had been reported and investigated by varying the length of terminal hydrocarbon tails, the type and length of the spacer, the symmetry of the molecule and the kinds of polar head group.[28,29]

Herein, a CO_2-responsive smart fluid was fabricated by mixing a gemini cationic surfactant (GCS) and its intermediate product (NDPO). Firstly, oleic acid and 3-dimethylaminopropylamine reacted to form a single-chain weak cationic surfactant with a tertiary amine head group – *N*-[3-(dimethylamino) propyl]oleamide (NDPO). Then, 1,3-dibromopropane was used as spacer to reacted with NDPO to form gemini cationic surfactant – trimethylene α,ω-bis(oleate amide propyl dimethyl ammonium bromide) (GCS). Because the quaternization of tertiary amine groups and brominated compounds had extremely high reactivity, we could control the ratio of single-chain weak cationic surfactants and gemini cationic surfactants conveniently by adjusting the molar ratio of NDPO and 1,3-dibromopropane.[30,31] And we found that the mixture surfactants of GCS and NDPO with the molar ratio of 7 : 3 approximately could be dissolved in water and form a uniform vesicle-containing solution with a low viscosity and a weak light transmission. After bubbling CO_2, the tertiary amines of NDPO was protonated to become cationic surfactants, and the solution showed an obvious gel–sol transition and a great increase in light transmittance as its self-assembly structure changed from vesicles to wormlike micelles. When the solid content of GCS/NPDO mixtures was higher than 5 wt% in solution, the sample treated by CO_2 behaved as a gel over a wide frequency range. In addition, the sol–gel transition could be repeatedly and reversibly switched by cyclically bubbling CO_2 and N_2. Our work found a convenient way to adjust the ratio of gemini cation surfactant/single-chain weak cationic surfactant mixtures, providing a new strategy for the design of CO_2-responsive smart fluids, providing some inspiration to find industrial uses such as CO_2 flooding in enhanced oil-recovery processes.

Experiment

Materials

Oleic acid, 3-dimethylaminopropylamine, 1,3-dibromopropane and ethanol were purchased from Sinopharm Chemical Reagent Co. Ltd. All the materials were used as received without further purification and experiments were performed using deionized (DI) water.

Synthesis and NMR characterization of the *N*-[3-(dimethylamino)propyl]oleamide (NDPO)

Oleic acid (141.23 g, 0.5 mol) was added to a four-necked flask, which was equipped with a reflux device, a thermometer, a dropping funnel and a nitrogen inlet, and then heated to 170 °C under N_2 atmosphere. 3-Dimethylaminopropylamine (76.635 g, 0.75 mol) was added dropwise to oleic acid over 4 hours. After the addition, the mixture kept stirring for 6 hours under 170 °C. Once the reaction was completed, the excess 3-dimethylaminopropylamine and water were distilled off under reduced pressure at 100 °C to obtain a yellowish liquid. (172.31 g, yield: 94%, the ^{1}H NMR spectrum is seen in Fig. S1a†)

Synthesis of the gemini cation surfactant (GCS)

The synthesis process of the gemini cation surfactant was illustrated in Fig. 1a. *N*-[3-(Dimethylamino)propyl]oleamide was dissolved in ethanol and added amount of 1,3-dibromopropane into the mixture. Gemini cation surfactant (GCS) – trimethylene α,ω-bis(oleate amide propyl dimethyl ammonium bromide) was obtained after reacting for 12 hours at 45 °C.

When the molar ratio of NPDO and 1,3-dibromopropane was 2 : 1, by titrating the amine value, we found that the conversion rate of this reaction could be close to 99%. Because the quaternization of tertiary amine groups and brominated compounds had extremely high reactivity, we could control the ratio of single-chain weak cationic surfactant and gemini cation surfactant by adjusting the ratio of NPDO and 1,3-dibromopropane. We named the CO_2-responsive smart fluid as G_X (where X represented the molar fraction of the GCS in the GCS/NDPO mixtures, n_{spacer} and n_{NDPO} represented the molar concentrations of 1,3-dibromopropane and *N*-[3-(dimethylamino)propyl]oleamide, respectively):

$$X = \frac{2n_{spacer}}{n_{NDPO}} \times 100\% \quad (1)$$

Characterization

Nuclear magnetic resonance proton spectroscopy (^{1}HNMR) was used to characterize the dry surfactant samples (Bruker AV300 nuclear magnetic resonance instrument). Deuterated DMSO was used as the nuclear magnetic solvent. The chemical shift of 0 ppm is tetramethylsilane TS, and the coupling constant unit is Hertz. It is calculated by Fourier transform mode. Dynamic light scattering (DLS) measurements were performed on

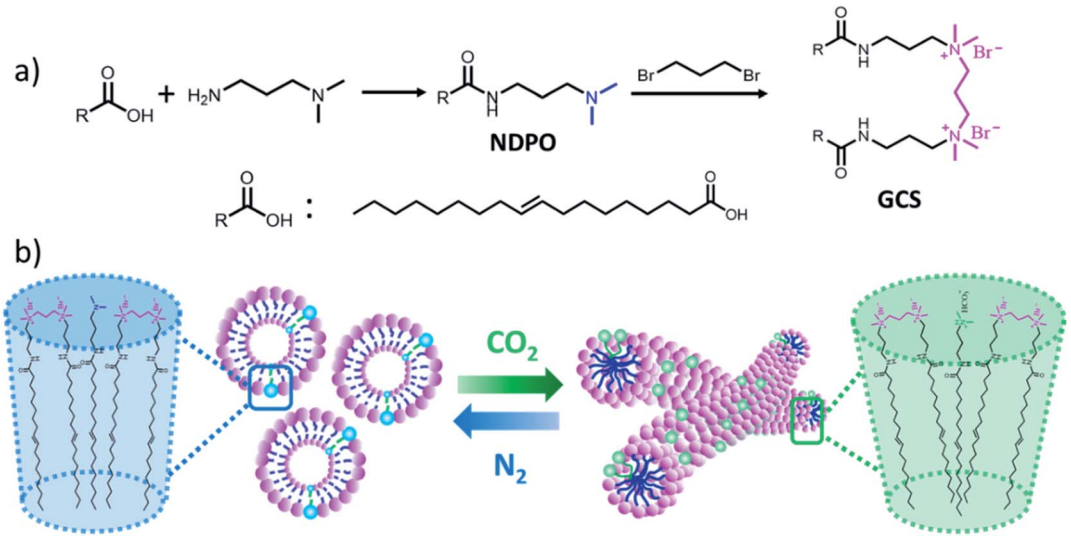

Fig. 1 The preparation process (a) and the switching mechanism (b) of the CO_2-responsive smart fluid.

a Brookhaven Instrument BI-200SM with a laser wavelength of 636 nm at 25 °C. The scattering angle was fixed at 90°. The DLS data was analysed with the software supplied by Brookhaven and the apparent hydrodynamic diameters of the micelles were obtained. The light transmittance test was measured by UV-vis spectrophotometer (Shimadzu UV1800). Deionized water was used as the blank sample, and the wavelength was selected from 200–800 nm.

Rheological measurements

Rheological measurements were conducted on an ARG2 stress controlled rheometer (TA AR-G2) at 25 °C using a cone-plate of 40 mm diameter with a cone angle of 4. The viscosity was measured as a function of shear rate for determining the zero shear viscosity. The storage modulus (G') and loss modulus (G'') were measured as a function of frequency within a linear viscoelastic regime, which was determined from the prior stress-sweep test. To investigate the self-healing properties of the samples in response to applied shear forces, the samples were placed between the para-plate and the platform with special care. The following programmed procedure (applied shear force, expressed in terms of strain; duration in parentheses) was used: 1% (300 s)/50% (200 s)/1% (300 s)/50% (200 s)/1% (300 s)/50% (200 s)/1% (300 s). During all measurements, a solvent trap was used to minimize water evaporation.

Cryo-TEM observation

The specimens for cryo-TEM observation were prepared in a controlled environment to vitrify the solutions. The temperature of the chamber was regulated between 25 and 28 °C, and the relative humidity was kept close to saturation to prevent evaporation during preparation. 5 μL of solutions pre-heated at 30 °C was placed on a carbon-coated holey film supported by a copper grid and gently blotted with a piece of filter paper to obtain a thin liquid film (20–400 nm) on the grid. Next, the grid was quenched rapidly into liquid ethane at −180 °C and transferred into liquid nitrogen (−196 °C) for storage.[27] The vitrified specimen stored in liquid nitrogen was then transferred to a Tecnai G2 F20 cryo-microscope. The acceleration voltage was 200 kV, and the working temperature was kept below −170 °C.

Results and discussion

Formation and characterization of the CO_2-responsive smart fluids

The preparation process of the CO_2-responsive smart fluid was illustrated in Fig. 1a. Firstly, the *N*-[3-(dimethylamino)propyl] oleamide (NDPO) was synthesized by amidation of oleic acid and 1,3-dimethylaminopropylamine. Then, we used 1,3-dibromopropane as spacer to link the *N*-[3-(dimethylamino)propyl] oleamide to form gemini cation surfactant (GCS) – trimethylene α,ω-bis(oleate amide propyl dimethyl ammonium bromide) (see Fig. S1† for the ^{1}H NMR spectrum of the NPDO and the GCS). During the second step of the reaction, the molar fraction of the GCS in all surfactants could be well controlled based on adjusting the ratio of 1,3-dibromopropane and NDPO. The switching mechanism of the CO_2-responsive smart fluid was illustrated in Fig. 1b. We inferred the introduction of CO_2 protonated the NDPO to be positively charged. To confirm this, ^{1}H NMR characterizations of the G_{70} sample with and without CO_2 were performed, and the spectra were compared in Fig. S2.† It could be seen that, after being treated with CO_2, the chemical shifts of $(CH_3)_2N$–CH_2–CH_2–, $(CH_3)_2N$–CH_2–CH_2–, and $(CH_3)_2N$–CH_2–CH_2– moved from 2.17 (a_1), 2.32 (b_1), and 1.66 (c_1) to 2.63 (a_2), 2.86 (b_2), and 1.99 (c_2) ppm, respectively, reflecting the protonation of the tertiary amine group in NPDO.[25]

For the CO_2-responsive smart fluid, the average packing parameter P (Israelachvili's packing parameter $P = v/al$, where l and v are the effective maximum length and volume of the hydrophobic tail, respectively, and a is the effective headgroup

area of per surfactant molecule constituting the aggregate[1]) of the GCS/NPDO mixtures in G_{70} sample should be 1/2–1, a typical value range of vesicles aggregates as indicated in Fig. 5a. After bubbling CO_2, the NPDO was protonated and positively charged. The electrostatic repulsion of the head-groups between GCS and protonated NPDO increased. This was equivalent to say that the effective head group area of protonated NPDO increased. The average packing parameter *P* of the GCS/NPDO mixtures in the presence of CO_2 decreased accordingly, inducing the transition of aggregate from vesicles into wormlike micelles.

Compared with single-chain weak cationic surfactants, gemini cation surfactants with two hydrophilic head groups and two hydrophobic long chains had better water solubility, higher surface activity, and better wetting properties. CO_2-responsive smart fluid with different molar fractions of GCS in the GCS/NDPO mixtures had many differences including light transmittance, hydrodynamic diameter, viscosity, and response capabilities to carbon dioxide. As showed in Fig. 2a, G_0 was a milky white solution with a yellow oily liquid floating on it, indicating that the solubility of NDPO was low. With the increase of molar fraction of gemini cation surfactants, the solution became transparent. G_{75} was obvious translucent and had bluish light, indicating the presence of large-sized particles in the solution. As the increase of fraction of GCS with positively charged quaternary ammonium head group, the electrostatic repulsion between the quaternary amine head group became bigger. It leaded to an increase in the effective contact area of the mixed surfactants, thus causing a decrease in the packing parameter. The surfactant packing parameter was decreased, so the arrangement of surfactant molecules was closer, which was more conducive to the formation of wormlike micelles.

So we further investigated the aggregation state of 2 wt% samples with different molar fractions (G_{60}, G_{65}, G_{70}, G_{75}, G_{80}, and G_{100}) through dynamic light scattering and light transmittance tests. In Fig. 2b, as the molar fraction of GCS increased, the light transmittance of 2 wt% samples increased significantly. However, in the small wavelength range, the light transmittance of the samples was very low, indicating that there might have hundreds of nanometre-scale self-assembly structure in the solution. As the DLS curves for a series of 2 wt% samples shown in Fig. S3,† when GCS molar fraction was low,

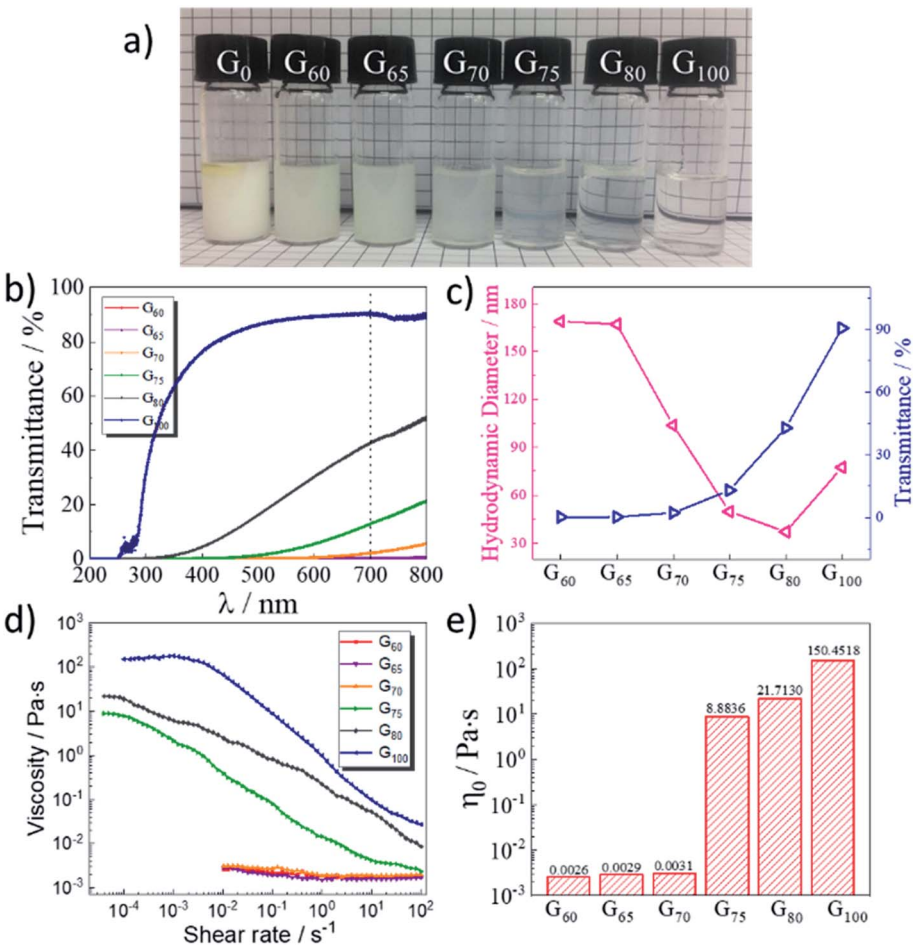

Fig. 2 (a) Photograph of 2 wt% samples with different molar fractions of the GCS in the GCS/NPDO mixtures (G_0, G_{60}, G_{65}, G_{70}, G_{75}, G_{80}, and G_{100}). (b) Light transmittance curves (The curves of G_{60} and G_{70} are very close to the *x*-axis due to their low light transmittances), (c) hydrodynamic diameters and light transmittances at 700 nm, (d) viscosity *versus* shear rate plots, and (e) zero-shear viscosity for 2 wt% samples with different molar fractions of the GCS in the GCS/NPDO mixtures (G_{60}, G_{65}, G_{70}, G_{75}, G_{80}, and G_{100}).

the DLS peak of the sample appeared between 100–500 nm, which was consistent with the size of general surfactant vesicle assemblies. When molar fraction of GCS increased, an integrated peak appeared at 1000 and 1000 nm, indicating that wormlike micelles might be formed.[32–34] In Fig. 2c, we showed the hydrodynamic diameter and the light transmittance at 700 nm of these samples, which indicated that increasing the conversion of GCS might induce the self-assembly structure of surfactants to transfer from vesicles to wormlike micelles. Especially from G_{70} to G_{75}, the light transmittance and hydrodynamic diameter of the samples had a significant change. Besides, the hydrodynamic size of G_{100} was almost double that of G_{80}. This phenomena might be caused by the increased distance of the entanglement length, *i.e.*, the average contour length between two entanglement points, which further demonstrated the formation of elongated wormlike micelles.[35]

Next, we studied the zero-shear viscosity of the above samples. From the viscosity behavior of the 2 wt% samples shown in Fig. 2d and e, it could be seen that the viscosity of G_{60}, G_{65}, and G_{70} was always in a low level. The zero-shear viscosity of G_{75} and G_{80} was 8.88 pa s and 21.71 pa s, respectively, and the viscosity decreased with the increase of shear rate. The zero-shear viscosity of G_{100} was obviously higher than other samples, its zero-shear viscosity reached 150 pa s, and the viscosity had a plateau at low shear rate, indicating that it was a relatively stable wormlike micelle solution.

CO_2-responsiveness of the 2 wt% G_{70} sample

In order to decrease the initial zero viscosity and increase the CO_2-responsive ability of the smart fluid, the amount of NDPO in GCS/NDPO mixtures should be as much as possible. However, with the increase of NPDO, the solubility of the system became poor. For the GCS/NDPO mixtures with the molarity ratio of 7 : 3, the uniform solution exhibited both a low viscosity and a little light transmission. Therefore, we selected G_{70} (molarity ratio of 7 : 3) as the representative sample to study. We first studied the transition of the light transmittance and hydrodynamic diameter of the 2 wt% G_{70} sample before and after the introduction of CO_2. Fig. 3a showed the change of light transmittance (200–800 nm) before and after the solution was exposed to CO_2. The introduction of CO_2 significantly increased the light transmittance of the system, which was consistent with the photographs inset in Fig. 3a. The solution was a low-viscosity liquid with blue light before the introduction of CO_2. After we bubbled CO_2, the solution became transparent, and the CO_2 bubbles could temporarily suspend in the solution, which indicated the viscosity increased. As the DLS curves of the hydrodynamic diameter of the 2 wt% G_{70} sample shown in Fig. 3b, the average hydrodynamic diameter of the surfactant self-assembly was 104 nm before the introduction of CO_2. After the introduction of CO_2, the average hydrodynamic diameter decreased to 39 nm, which was consistent with the change of the vesicles into wormlike micelles in particle size.

In order to further investigate the CO_2 response performance of the 2 wt% G_{70} sample, we tested the rheological properties before and after the introduction of CO_2. From the Fig. 4a and b, we clearly observed the increasing of viscosity and modulus after the introduction of CO_2. As shown in Fig. 4a, before

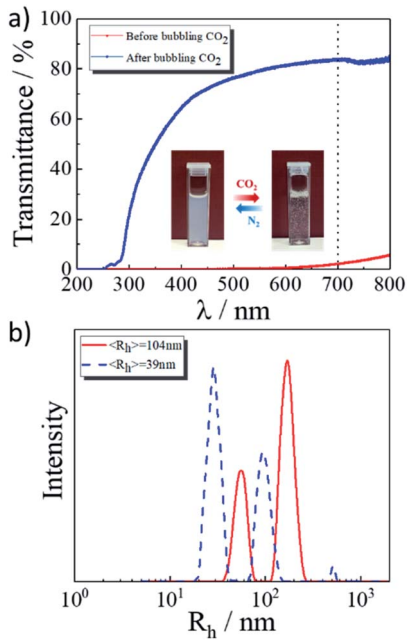

Fig. 3 (a) Light transmittance curves and snapshots for 2 wt% G_{70} sample before and after bubbling CO_2. (b) Intensity weighted distribution of apparent hydrodynamic diameters for 2 wt% G_{70} sample before and after bubbling CO_2.

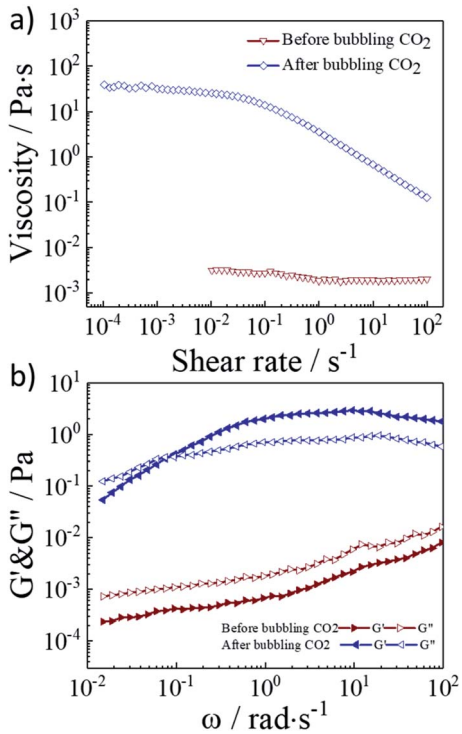

Fig. 4 (a) Viscosity *versus* shear rate plots, and (b) linear viscoelastic modulus, *G′* and *G″* for 2 wt% G_{70} sample before and after bubbling CO_2.

bubbling CO_2, the viscosity of the solution was about 3 mpa s, which was close to the viscosity of pure water and independent of the shear rate. After the solution was exposed to CO_2, the zero-shear viscosity of the system increased by 4 orders of magnitude. In the shear range of 10^{-4}–10^{-1} s^{-1}, the viscosity appeared a plateau, and then it showed shear thinning with the increase of shear rates. We inferred that the introduction of CO_2 would drive the self-assembly from vesicles to worm-like micelles. The worm-like micelle cross-linking network relied on physical interaction forces and could maintain stability at small shear rates, but as the increase of shear rate, the cross-linking network would be destroyed, leading to a decrease in the viscosity. Fig. 4b showed the frequency sweep curves of the storage modulus G' and the loss modulus G'' of the 2 wt% G_{70} sample. Before the introduction of CO_2, the G' of the sample was less than the G'' over the entire frequency range, which appeared an obvious characteristics of Newtonian liquid behavior. After bubbling CO_2, the G' of the solution was less than the G'' in the low frequency range, and greater than the loss modulus G'' in the high frequency range. The intersection of G' and G'' appeared the sample with CO_2 was likely as a sticky elastic fluid. The change in storage modulus G' and loss modulus G'' also corresponded to the self-assembly transition from vesicles to worm-like micelles.

To confirm the morphology of the self-assemblies of GCS/NPDO mixtures in solution, the 2 wt% G_{70} samples were further observed by cryo-TEM. The results were shown in Fig. 5a. It could be seen that the size of the vesicles ranged from tens to hundreds of nanometers. This could explain the existence of multiple peaks in the DLS of G_{70} sample as shown in Fig. 3b. In the presence of CO_2, the elongated, flexible wormlike micelles formed and entangled with each other as shown in Fig. 5b. These threadlike aggregates had a diameter of several nanometers and a length in the micrometer range. Therefore, the dramatic rheological change observed in G_{70} sample could be clearly ascribed to the transition of aggregates from vesicles to an entangled network of wormlike micelles after bubbling CO_2.

Reversibility of CO_2-induced gelation

As a green trigger, CO_2 could lead to many switching cycles without the accumulation of by-products.[36] Thus, we evaluated the reversible switch ability in rheological behaviours. As shown in Fig. 6a, the light transmittance of the smart fluid could be repeatedly and reversibly switched upon alternately bubbling CO_2 and N_2. For more than four cycles, the changes in the light transmittance were detected without any deterioration. On the other hand, Fig. 6b showed variation of the zero-shear viscosity values of the invertible smart fluid during four cycles, which further confirms the perfect reversible ability of the CO_2 response behavior. In the presence of CO_2, the tertiary amine group of NDPO was protonated and became positively charged, leading to an increase in the effective contact area of the hydrophilic head groups. As a result, the average packing parameter of the mixed surfactants in G_{70} sample decreased accordingly. It drove the self-assembly structure transfer from vesicles to worm-like micelles. Bubbling N_2 into the sample, or heating the sample to discharge CO_2, it could return to the initial state.

Self-healing study of the 5 wt% G_{70} sample with CO_2

When the solid content of GCS/NPDO mixtures was higher than 5 wt% in solution, the sample with CO_2 behaved as a gel over a wide frequency range. In order to better study the rheological properties and self-healing properties of the G_{70} sample, we

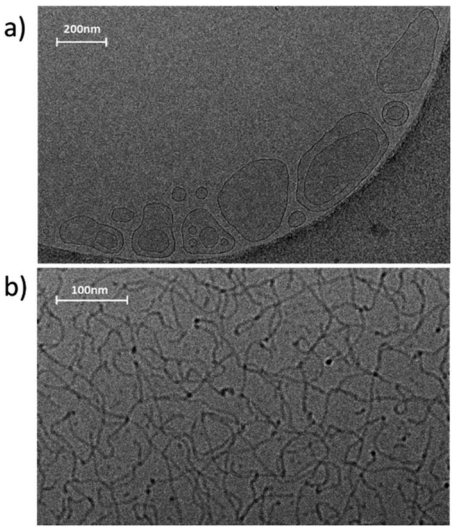

Fig. 5 Cryo-TEM images of the 2 wt% G_{70} sample (a) before and (b) after bubbling CO_2 (the dark part in the lower right corner in (a) is copper grid). The scale bars are (a) 200 nm and (b) 100 nm.

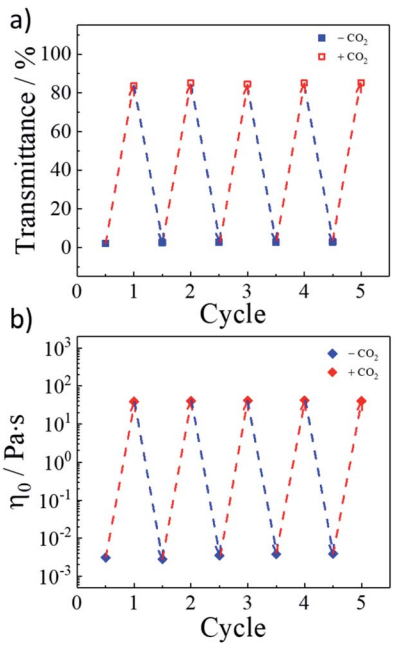

Fig. 6 Reversible switchability of (a) light transmittance at 700 nm and (b) light transmittance for the 2 wt% G_{70} sample upon alternate treatment of CO_2 and N_2.

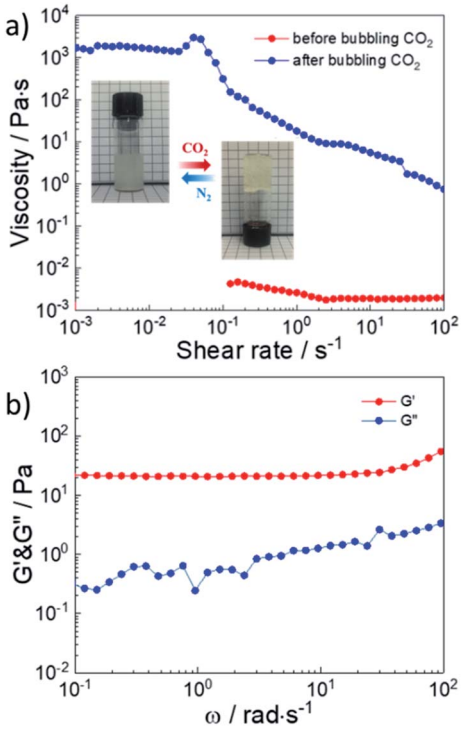

Fig. 7 (a) Viscosity *versus* shear rate plots and snapshots for 5 wt% G_{70} sample before and after bubbling CO_2. (b) Linear viscoelastic modulus, G' and G'', for 5 wt% G_{70} sample after bubbling CO_2.

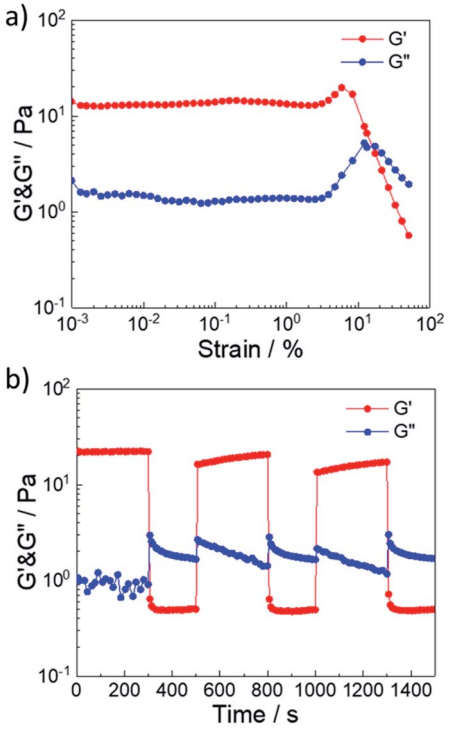

Fig. 8 (a) Modulus–strain curves and (b) repeated dynamic strain step tests (γ = 1% or 50%) for 5 wt% G70 sample after bubbling CO_2.

increased the solid content of GCS/NPDO mixtures from 2 wt% to 5 wt% to ensure that the G_{70} sample could maintain good strength after the introduction of CO_2. The CO_2-response performance of 5 wt% G_{70} sample was shown in Fig. 7a. After CO_2 was introduced, the zero-shear viscosity of the system was increased by 6 orders of magnitude. The inset photographs demonstrated the CO_2-responsive sol–gel transition. Turning the bottle over, the position and shape of the hydrogel in the bottle had not changed, which showed that the hydrogel had good strength and viscosity to support its own weight. Moreover, we performed a frequency scan on the storage modulus G' and the loss modulus G'' of the 5 wt% G_{70} sample after the introduction of CO_2 as shown in Fig. 7b. The storage modulus G' of the system was always greater than the loss modulus G'' over the entire frequency range, quantitatively proved that the system did behave as a gel after CO_2 introduction. The loss modulus G'' had obvious frequency dependence, indicating that the cross-linking network of the system was dynamic and formed based on physical interactions. Therefore, the 5 wt% G_{70} sample was CO_2-responsive smart fluid and behaved like a hydrogel after the introduction of CO_2 over a wide frequency range.

Next, we investigated the self-healing properties of 5 wt% G_{70} sample with CO_2.[37–39] First, a strain sweep measurement was conducted on the 5 wt% G_{7O} sample with CO_2 to test the influence of the strain. As depicted in Fig. 8a, G' was larger as G'' (elastic-dominating) under small strain (γ < 5%). And the values of G' and G'' kept constant, suggesting that the hydrogel network remained unaffected due to the intact cross-linkages. While the strain kept increasing, a sol–gel transition point (γ = 15.5%) occurred, implying that the hydrogel network was destroyed due to the disassociation of the cross-linkages at a high deformation strain. Finally, repeated dynamic strain step tests (γ = 1% or 50%) were carried out in Fig. 8b. It could be seen that a 50% strain could completely inverted the G' and G'' values, indicating the deconstruction of the network. By returning the strain to 1%, G' and G'' recovered their original values rapidly, indicating the quick recovery of wormlike micelles. During the cyclic tests, this recovery behavior was significantly reversible. When the concentration of worm-like micelles increased, the worm-like micelles formed a three-dimensional network structure, and a sol–gel transition occurred macroscopically. The three-dimensional network structure formed by worm-like micelles was dynamic physical cross-linking, and would be destroyed by stress. After the stress was withdrew, the structure would be restored to the original state spontaneously, showing excellent self-repairing performance. Therefore, the 5 wt% G_{70} sample with CO_2 exhibited the significant self-healing property within a short period of time.

Conclusions

In summary, we designed a CO_2-responsive smart fluid based on supramolecular assembly structures varying from vesicles to wormlike micelles. The mixtures of gemini cation surfactants and single-chain weak cationic surfactants, GCS/NDPO, with the molarity ratio of 7 : 3 approximately could form vesicles in

aqueous solution by supramolecular self-assembly. In the presence of CO_2, the single-chain weak cationic surfactants NDPO with tertiary amine head groups were protonated due to the acidity of the carbonic acid. As a result, the effective contact area of the hydrophilic head groups increased and the packing parameter decreased. This induced the self-assembly structures of GCS/NDPO mixtures changed from vesicles to worm-like micelles. The zero-shear viscosity of solution, therefore, increased more than four orders in magnitude. When the gemini cation surfactant accounted for 70%, its self-assembly structures changed from vesicles to worm-like micelles after bubbling CO_2. When the surfactant concentration was higher than 5 wt%, the G_{70} sample in the presence of CO_2 behaved as a gel over a wide frequency range and exhibited the shear thinning and self-healing properties. The sol–gel transition could be adjusted repeatedly and reversibly by cyclically bubbling CO_2 and N_2 without causing cumulative damage to the system by-products. We believe that this work will provide a general and simple strategy for the design of CO_2-responsive smart fluids, fostering their practical application in a number of fields such as CO_2 flooding in enhanced oil-recovery processes.

Conflicts of interest

There are no conflicts to declare.

Acknowledgements

This work was supported by the National Science and Technology Major Project of the Ministry of Science and Technology of China (2016ZX05016), and the National Science and Technology Major Project of the Ministry of Science and Technology of China (2016ZX05046).

Notes and references

1 Z. Chu, C. A. Dreiss and Y. Feng, *Chem. Soc. Rev.*, 2013, **42**, 7174–7203.
2 P. Theato, B. S. Sumerlin, R. K. O'Reilly and I. I. I. T. H. Epps, *Chem. Soc. Rev.*, 2013, **42**, 7055–7056.
3 M. A. C. Stuart, W. T. S. Huck, J. Genzer, M. Müller, C. Ober, M. Stamm, G. B. Sukhorukov, I. Szleifer, V. V. Tsukruk, M. Urban, F. Winnik, S. Zauscher, I. Luzinov and S. Minko, *Nat. Mater.*, 2010, **9**, 101–113.
4 J. Hao and H. Hoffmann, *Curr. Opin. Colloid Interface Sci.*, 2004, **9**, 279–293.
5 Y. Qiao, Y. Lin, Z. Yang, H. Chen, S. Zhang, Y. Yan and J. Huang, *J. Phys. Chem. B*, 2010, **114**, 11725–11730.
6 J.-M. Lehn, *Science*, 2002, **295**, 2400–2403.
7 T. J. Deming, *Soft Matter*, 2005, **1**, 28–35.
8 Y. Zhang, M. Gao, Q. You, H. Fan, W. Li, Y. Liu, J. Fang, G. Zhao, Z. Jin and C. Dai, *Fuel*, 2019, **241**, 442–450.
9 Y. Liu, P. G. Jessop, M. Cunningham, C. A. Eckert and C. L. Liotta, *Science*, 2006, **313**, 958–960.
10 Y. Zhao, P. Cheung and A. Q. Shen, *Adv. Colloid Interface Sci.*, 2014, **211**, 34–46.
11 H. Shi, Y. Wang, B. Fang, Y. Talmon, W. Ge, S. R. Raghavan and J. L. Zakin, *Langmuir*, 2011, **27**, 5806–5813.
12 Y. Qiu and K. Park, *Adv. Drug Delivery Rev.*, 2001, **53**, 321–339.
13 X. Sun, X. Liu, C. Li, Y. Wang, L. Liu, F. Su and S. Li, *J. Appl. Polym. Sci.*, 2018, **135**, 45732.
14 H. Cabral, M. Nakanishi, M. Kumagai, W.-D. Jang, N. Nishiyama and K. Kataoka, *Pharm. Res.*, 2009, **26**, 82–92.
15 H. Yan, Y. Long, K. Song, C.-H. Tung and L. Zheng, *Soft Matter*, 2014, **10**, 115–121.
16 Y. Lin, Y. Qiao, Y. Yan and J. Huang, *Soft Matter*, 2009, **5**, 3047–3053.
17 Z. Chu and Y. Feng, *Chem. Commun.*, 2010, **46**, 9028–9030.
18 Y. Zhang, Y. Feng, J. Wang, S. He, Z. Guo, Z. Chu and C. A. Dreiss, *Chem. Commun.*, 2013, **49**, 4902–4904.
19 J. H. Park, B. D. Chin and O. O. Park, *J. Colloid Interface Sci.*, 2001, **240**, 349–354.
20 T. Sakakura, J.-C. Choi and H. Yasuda, *Chem. Rev.*, 2007, **107**, 2365–2387.
21 D. Han, X. Tong, O. Boissière and Y. Zhao, *ACS Macro Lett.*, 2012, **1**, 57–61.
22 Y. Zhang, W. Kong, P. An, S. He and X. Liu, *Langmuir*, 2016, **32**, 2311–2320.
23 G. Zhao, X. Wu, R. Luan, S. Azizullah, H. Fan and C. Dai, *J. Mol. Liq.*, 2019, **274**, 133–139.
24 X. Wu, Y. Huang, S. Fang, C. Dai, H. Li, Z. Xu and M. Zhao, *J. Ind. Eng. Chem.*, 2018, **60**, 348–354.
25 Y. Zhang, Y. Feng, Y. Wang and X. Li, *Langmuir*, 2013, **29**, 4187–4192.
26 Y. Zhang and Y. Feng, *J. Colloid Interface Sci.*, 2015, **447**, 173–181.
27 Y. Zhang, Z. Chu, C. A. Dreiss, Y. Wang, C. Fei and Y. Feng, *Soft Matter*, 2013, **9**, 6217.
28 B. Sekhon, *Resonance*, 2004, **9**, 42–49.
29 S. Hait and S. Moulik, *Curr. Sci.*, 2002, **82**, 1101–1111.
30 N. Pal, N. Saxena and A. Mandal, *Colloid Polym. Sci.*, 2017, **295**, 2261–2277.
31 X. Wu, C. Dai, S. Fang, H. Li, Y. Wu, X. Sun and M. Zhao, *Phys. Chem. Chem. Phys.*, 2017, **19**, 16047–16056.
32 H. Liu, W. Wang, H. Yin and Y. Feng, *Langmuir*, 2015, **31**, 8756–8763.
33 L. Chen, T. Chen, W. Fang, Y. Wen, S. Lin, J. Lin and C. Cai, *Biomacromolecules*, 2013, **14**, 4320–4330.
34 Z. Iatridi and C. Tsitsilianis, *Chem. Commun.*, 2011, **47**, 5560–5562.
35 X. Su, M. F. Cunningham and P. G. Jessop, *Chem. Commun.*, 2013, **49**, 2655–2657.
36 C. Xiong, K. Peng, X. Tang, Z. Ye, Y. Shi and H. Yang, *RSC Adv.*, 2017, **7**, 34669–34675.
37 Y. Yang and M. W. Urban, *Chem. Soc. Rev.*, 2013, **42**, 7446–7467.
38 U. Gulyuz and O. Okay, *Soft Matter*, 2013, **9**, 10287–10293.
39 H. Liu, C. Xiong, Z. Tao, Y. Fan, X. Tang and H. Yang, *RSC Adv.*, 2015, **5**, 33083–33088.

